Journal of Computational Interdisciplinary Sciences (2008) 1(1): 11-32

ISSN 1983-8409
http://epacis.org

Pattern formation in spatially ramped Rayleigh-Bénard systems

José Pontes[1,2*], Daniel Walgraef[1] and Christo I. Christov[3†]

Manuscript received on July 25, 2008 / accepted on October 18, 2008

ABSTRACT

We study pattern formation and selection in Rayleigh-Bénard systems confined between well conducting horizontal boundaries and subjected to a weak horizontal gradient of the Rayleigh number. The study is based on the numerical integration of the Swift-Hohenberg equation and addresses the questions of the preferred orientation of the patterns with respect to the gradient of the Rayleigh number, boundary effects observed at subcritial sidewalls, the characteristics of long-term evolution of the patterns with emphasis on the wavelength selection, and the effect of non-potential modifications of the Swift-Hohenberg equation.

It is shown that, contrary to common belief, the rolls do not align with the direction of the horizontal temperature gradient (Dewel, 1989; Malomed, 1993), due to the influence of the walls. Rather, rolls approach a sidewall perpendicularly when the local bifurcation parameter is sufficiently beyond the threshold but tend to be parallel to a subcritical or critical sidewall. Simulations performed with non-potential modifications of the Swift-Hohenberg equation lead in most cases, to asymptotic time-dependent behaviours.

Keywords: Rayleigh-Bénard convection, Pattern Formation, Nonlinear Systems, Temperature gradients.

[1]Center for Nonlinear Phenomena and Complex Systems, CP–231, Université Libre de Bruxelles, B–1050 Brussels, Belgium.

[2]Promon Engenharia Ltda, Praia do Flamengo, 154, 22210-910 Rio de Janeiro, RJ, Brazil.

[3]Instituto Pluridisciplinar, Universidad Complutense, Paseo Juan XXIII, 1, E–28040 Madrid, Spain.

*Present address: Metallurgy and Materials Engineering Department, Federal University of Rio de Janeiro, P.O. Box 68505, 21941-972 Rio de Janeiro, RJ, Brazil.

†Present address: Department of Mathematics, University of Louisiana at Lafayette, Lafayette, LA 70504-1010, USA.

1 INTRODUCTION

The problem of thermal convection in a thin layer of fluid heated from below has been widely studied in the last hundred years. After Bénard's experiment and the theoretical explanation proposed by Lord Rayleigh, the works released during the first part of the 20th century were dedicated to understanding why and when a transition from the homogeneous to the structured state occurs. Details and reviews on the results obtained in this phase are found for instance, in the works of Chandrasekhar (1961) and Normand et al. (1977). The following step, concerning the saturation mechanism of the instability, goes back to the work of Landau (1944), who added a nonlinear term to the original equation, to cope with the nonlinear satruration beyond the critical point. A review of the underlying saturation mechanism can be found in the work by Velarde et al. (1980). The problem of pattern selection and stability in Rayleigh-Bénard convection has been extensively studied in the last fifty years and these studies have been closely linked to the development of nonlinear methods. Of particular importance are the works of Swift and Hohenberg (1977), who obtained an equation for an order parameter-like, which describes the evolution of complex patterns in extended systems.

In this work (Peaceman and Rachford Jr. 1955) we analyze a problem that has received less attention: the problem of pattern formation and selection in non-uniformly forced systems. Among the existing literature on the subject, we may cite the work of Kelly and Pall (1976), who derived the form of the base state of the problem, the experimental work of Srulijes (1979) and two articles by Walton (1982, 1983). The first one, is devoted to the derivation of the $(1+1)D$ amplitude equation for a structure of rolls and also, to finding a solution that asymptotically matches the system behaviour in the supercritical region and that decays in the subcritical region. The second one deals with the preferred orientation of rolls close to a subcritical wall. We may also cite the work of Dewel et al. (1989), concerning the orientation of rolls in ramped systems.

We consider a Boussinesq fluid confined between insulating rigid sidewalls and good conducting horizontal boundaries, submitted to a weak gradient of temperature in the lower surface. Patterns formed under these conditions result from the competition between four major effects: the bias introduced by the initial condition, the system size, bulk and boundary effects. Initial conditions are rarely uniform, due to external perturbations to which the system is always submitted. For instance, random initial conditions induce the growth of modes with different orientation, during early stages of formation of the structure (Greenside 1984; Manneville 1990). Some modes tend to dominate all others in limited regions, while the structure evolves towards the steady state. When nonlinear effects saturate the growth, a structure with regions or domains often emerges (Manneville and Pomeau 1983; Malomed et al. 1990), provided that the system is large enough. By "large" we mean a system where the horizontal length L, measured in number of system heights, is large when compared with the *coherence length* $(\xi/\sqrt{\varepsilon})$ (Manneville 1990), which is the characteristic length in which the modulation occurs. Here, ξ is the system length, measured in number of system thicknesses and ε is the supercriticality level.

Bulk effects tend to produce uniform structures with straight parallel rolls (Cross 1982) and uniform amplitude. The existence of a temperature gradient in the lower surface of the system determines a preferential direction for the structure, with rolls aligned palallel to the gradient (Dewel et al. 1989; Malomed et al. 1993).

System boundaries introduce conflicting requirements, by requesting rolls to bend across the convection cell, in order to perpendicularly approach sidewalls (Cross 1982). Furthermore, the amplitude must vanish at those walls (Brown and Stewarson 1977; Wesfreid 1978). In the case of uniform and moderately forced square systems, the interaction of these effects and the existence of a long coherence length often lead to a pattern characterized by a pair of focuses located in diagonally opposite corners. There is a symmetry with respect to the diagonal (Fig. 1a). In the opposite case of strongly forced systems, short coherence lengths lead to the "fusion" of the pattern (Walgraef 1997) and to labirynth structures (Fig. 1b).

Much less is known about subcritical boundary effects, since they do not appear in uniformly forced systems. Indeed, systems forced with a horizontal gradient of the Rayleigh number undergo an imperfect bifurcation (Walton 1982) that allows for a weak structure in the subcritical region and we can argue wheather boundary effects are similar as in uniformly forced systems. Walton (1983) was the first to adress the problem. He assumed a ramped system in which the Rayleigh number attains its maximum at a sidewall and considered the relative stability of parallel and perpendicular rolls to that wall. Two cases were identified: if the wall temperature is sufficiently above the critical point, rolls perpendicular to the wall prevail. In the opposite case, where the wall was still subcritical or even slightly supercritical, parallel rolls to the wall appear, induced by the non-trivial base state. The existence of this subcritical structure had already been experimentally identified by Srulijes (1979) and Kirchartz (1983) and also decteted in numerical simulations conducted by De Wit (1993) in the framework of a model for chemical systems.

(a) *(b)* *(c)*

Figure 1 – Patterns obtained in uniformly forced systems, by integration of the Swift-Hohenberg equation in square boxes, with rigid boundary conditions, $u = \partial u/\partial n = 0$, and starting from random initial conditions. (a): a structure displaying five *grains* in a 50×50 square, forced with $\varepsilon = 0.25$, and obtained at $t = 85000$. There is one grain perpendicular to each sidewall and one in the center of the system, which accounts for the transition between grains adjacent to the walls. The numerical grid contains 202 points. (b): pattern obtained at $t = 50000$, with the same parameters, except the forcing applied to the system, which is now $\varepsilon = 0.5$. The higher forcing results in a smaller *coherence length*, which allows the system to develop a structure with higher density of defects. (c): pattern obtained at $t = 10000$, in a 30×30 square, forced with $\varepsilon = 0.5$. Despite of the high forcing, the development of a more complex pattern, as found in (b), is inhibited by the smaller system size. The numerical grid contains 122 points.

Several questions remained unanswered: Srulijes experiments were conducted in a small system submitted to a strong gradient of the Rayleigh number and Walton considered a system subcritical in the bulk and unbounded in the direction of the wall. Furthermore, the roll parallel to the subcritical wall found by De Wit does not originate from a baroclinic motion. The following steps, devoted to further investigation of the origin of this effect and to the interactions between subcritical and supercritical patterns had not been accomplished to the present date.

The purpose of this work is to clarify some of these questions. The problem may be studied via two complimentary approaches. The first one (Pontes 1994) is based on amplitude equations for a structure containing one, two or three modes with arbitrary specified direction, generalizing Walton's result. Expressions and numerical values of the coefficients have been computed for some values of the Prandtl number, and numerical solutions were obtained and analyzed for small horizontal Rayleigh number gradients and a maximum of three interacting modes. In this case, two-dimensional simulations indicate that the system develops a structure with three domains. The first one comprises the bulk of the system, where the mode which best complies with the requirement of being parallel to the Rayleigh number gradient is the only one to survive. The two other domains are parallel to the gradient boundary layers, where the mode which best fits the condition of being perpendicular to the walls dominates. The third mode decays everywhere in the system. In addition, we found a weak structure of rolls parallel to the subcritical wall.

These results not only suggest that domains may develop in amped systems, but also, that more complex patterns may eventually appear, if the system is allowed to freely select the local orientation of the wavevector. However, such an analysis would require, in the framework of amplitudfe equations, that a PDE be written for each possible mode, leading to an excesively large sysem of equations. In order to overcome this dificulty, simplified versions of the original hydrodynamic equations that preserve the asymptotic properties of the dynamics and lead to the same amplitude equations obtained from the original evolution laws, have been used to analyze uniformly forced systems. The most popular one, obtained by projecting the Boussinesq equations on the critical modes of the system, assumed as a fluid with infinite Prandtl number and confined between well conducting stress-free boundaries is the well-known Swift-Hohenberg equation (1977).

Hence, the second approach to the problem that we present here is based on the study of such equations. In particular, Section 2 is devoted to the study of pattern formation by numerical integration of the Swift-Hohenberg equation adapted to spatially ramped systems. Section 3 adresses the problem of subcritical boundary effects in ramped systems. The numerical characterization of the asymptotic time evolution of the patterns is dicussed in Section 4, while the effect of localized forcings is illustrated in Section 5. Wavelength selection is discussed in Section 6. Comparisons with other works and results obtained with generalizations of the Swift-Hohenberg equation are presented in Sections 7, 8 and 9. Section 10 summarizes the results and discusses open

questions, while details of the numerical procedure may be found in the appendix.

2 THE ANALYSIS THROUGH THE SWIFT-HOHENBERG EQUATION

We study the following dynamical model which represents the dynamics of a Rayleigh-Bénard system with a horizontal temperature gradient in the x-direction, in the case of a Boussinesq fluid with infinite Prandtl number confined in a box with rigid sidewalls and good conducting horizontal boundaries.

$$\tau_0 \frac{\partial u}{\partial t} = \varepsilon u - g\, u^3 - \xi^4 \left(\nabla^2 + \kappa_0^2\right)^2 u \qquad (1)$$

Two variants of this model were also analyzed. The first one describes systems with mixed horizontal boundary conditions and reads:

$$\begin{aligned} \tau_0 \frac{\partial u}{\partial t} \;=\; & \varepsilon u - g\, u^3 + \nu\, u \left(\frac{\partial u}{\partial x} + \frac{\partial u}{\partial y}\right) \\ & - \xi^4 \left(\nabla^2 + \kappa_0^2\right)^2 u \end{aligned} \qquad (2)$$

The second one is the generalization to spatially ramped systems of a model studied by Greenside and Coughram Jr. in the case of horizontally uniform conditions, and reads:

$$\tau_0 \frac{\partial u}{\partial t} \;=\; \varepsilon u + 3\,|\nabla u|^2\, \nabla^2 u - \xi^4 \left(\nabla^2 + \kappa_0^2\right)^2 u \qquad (3)$$

where $\tau_0 = 0.0509$, $g = 1.29$ and $\xi^4 = 0.015$.

Here, we present first the results obtained by the numerical integration of the Swift-Hohenberg equation in horizontally finite systems, sufficiently large to allow the modulation of the structure. We tried to assess the influence of the system geometry on the pattern selection process to distinguish between situations, where the whole system is under supercritical conditions and situations, where the temperature gradient divides the system into a subcritical and a supercritical region, and to compare the results with those obtained in uniformly forced systems (cf. Fig. 1). As a result, our numerical simulations may be classified in four groups:

1. Simulations in square geometries, starting from random initial conditions, with the maximum of the bifurcation parameter set to $\varepsilon_{\max} = 0.5$ and assigned to the right wall of the system ($x = L$). The critical point was set to $x = L/2$, $x = 0$ and $x = -L$. The simulation of systems uniformely forced were run with $\varepsilon = 0.25$.
2. Same as in the previous case, but with $\varepsilon_{\max} = 1.0$. The simulation of systems uniformely forced were run with $\varepsilon = 0.50$.
3. Simulations in rectangular geometries, starting from random initial conditions, performed with a ramp $d\varepsilon/dx = 0.1$ and the critical point in $x = L/2$, in $x = 0$ and in $x = -L/2$. The simulation of systems uniformely forced were run with $\varepsilon = 0.01$.
4. Simulations of the Swift-Hohenberg with a quadratic convective-like term in the form $\nu\, u\, (\partial u/\partial x + \partial u/\partial y)$.
5. Simulations of the Swift-Hohenberg with a the cubic term in the form $3\,|\nabla u|^2\, \nabla^2 u$.

A sketch of the numerical method may be found in the appendix. An important question in this problem concerns the long term evolution of the pattern, and the identification of whether the system evolves towards, or has reached a steady state, or if the asymptotic state is unsteady. One is thus faced with the pratical problem of ascertaining when a pattern still evolves, if further qualitative changes are likely to occur due to the possible creation or anihilation of cells, to the climbing or gliding of dislocations, to the anihilation of entire grains, or rather, if we can, with reasonable confidence, expect that only minor adjustments, possibly in the phase of the pattern, would eventually occur. In the latter case, the pattern may be considered at the steady state, and the simulation process may be stopped. To do so, we have chosen a convergence criterion which is sensitive not only to the growth of the amplitude, but also to the evolution of the phase (Pontes 1994). The decision of further proceeding with a simulation or not is taken on monitoring the rate of change of the distance between two successive system states. Furthermore, in order to quantifie how "extended" a system is, we use a factor F, defined by Eq. 4, which is the ratio between the aspect ratio (the geometric "length" of the system) and the coherence length of the pattern (the characteristic length in wich modulation occurs).

$$F \;=\; \frac{L}{\xi/\sqrt{\varepsilon}} \qquad (4)$$

Here, L is the larger horizontal dimension of the system, expressed in number of system thicknesses and $\xi^4 = 0.015$, is the coefficient of the term $\xi^4 \left(\nabla^2 + \kappa_0^2\right)^2 u$ in the Swift-Hohenberg equation. The term $\xi/\sqrt{\varepsilon}$ defines the *coherence length* (see Table 1). The main results of the numerical simulations made by numerical integration of the Swift-Hohenberg equation (Eq. 1) are analyzed in the following sections.

Table 1 – The factor F (Eq. 4) in uniformly forced systems.

squares ($\varepsilon = 0.25$)	F	squares ($\varepsilon = 0.50$)	F	rect. ($\varepsilon = 0.10$)	F
20×20	28.6	20×20	40.4	20×10	18.1
30×30	42.9	30×30	60.6	20×30	27.1
40×40	57.1	40×40	80.8	20×50	45.2
50×50	71.4	50×50	101		

3 THE SUBCRITICAL BOUNDARY EFFECT IN RAMPED SYSTEMS

An inspection of the numerical results shown in Figs. 2, 3 and 4 reveals that except in a few cases, the ramped systems do not develop a structure of rolls parallel to the gradient, a fact observed in Srulijes experiments conducted in small boxes, and in the numerical integration of the amplitude equations performed by Hoyle (1995). The aligning effect of the gradient is dominating by the boundary effects. Nevertheless, ther is a qualitative difference between patterns formed in ramped systems and in uniformly forced systems: ramped systems, holding a subcritical region or, at least one sidewall where the bifurcation parameter does not exceed the critical value, display patterns with *one* single focus, usually located in the wall where the bifurcation parameter attains the maximum, whereas uniformly and moderately forced systems tend to develop a *pair* of focuses in the extremes of one of the diagonals of the box. The difference can be better observed in Figs. 2 and 4, where the forcing applied to the systems is sufficiently weak to induce the development of patterns with a low density of defects. The reason for the qualitative difference is a boundary effect that occurs close to critical or subcritical sidewall: the rolls tend to become parallel to these walls. The consequence of this effect in square or rectangular systems is that if rolls are parallel to one of the walls they are automatically perpendicular to the adjacent walls, and a focus is no longer required, because the system is not requested to develop rolls perpendicullar to all sidewalls. The resulting pattern contains a lower density of defects than those obtained in uniformly forced systems. We observed this effect irrespectively of the direction of the rolls in the supercritical region, the system geometry, the ramp configuration and the type of initial conditions.

Furthermore, this effect still appears in systems with a slightly supercritical sidewall, for instance, in the simulations of rectangular systems forced with a ramp $0.1 \leq \varepsilon \leq 0.3$. The second focus gradually returns as the whole system becomes supercritical. Figure 5 illustrates the effect, with three patterns obtained in systems containing a subcritical region. In each we case we show, on the left, an image of the pattern constructed with a linear scale of grays, and, on the right, an image of the same pattern constructed with a scale that enhances the weak structure existing in the subcritical region. In (a), we show the structure developed in a 20×20 square forced with a ramp $-1 \leq \varepsilon \leq 1$ along the x-direction, and starting from random iitial conditions. The right image shows the rolls parallel to the subcritical sidewall. In (b), we show the pattern obtained in the same geometry, forced with a ramp $-0.5 \leq \varepsilon \leq 0.5$ and starting from a structure of critical rolls parallel to $\mathbf{grad}\, u$. The amplitude of the initial condition is $A = 0$ in the subcritical region, and $A = \sqrt{\varepsilon/g}$ in the supercritical region. Despite of the initial condition and of the orientation of the supercritcal structure, the rolls bend and become parallel to the subcritcal sidewall. In (c), we show the pattern obtained in a 20×50 rectangle forced with a ramp $-0.1 \leq \varepsilon \leq 0.1$ starting from random initial conditions. The subcritical boundary effect is clearly present also in this case.

Figures 2, 3 and 4 show that in a very few cases the system develops a structure of rolls parallel to the ramp. An analysis of the time-evolution of one of these cases, shown in Fig. 6, suggests that even in this case, the asymptotic state is strongly influenced by the subcritical boundary effect: the system initially develops a focus that stands between $t \approx 150$ and $t \approx 1000$. After that, the focus slowly moves to the subcritical region and disapears at $t \approx 3000$. The structure aligns with the ramp. The same time-evolution is shown again in Fig. 7, where the images were constructed with a nonlinear scale of grays, in order to enhance the subcritical structure. This sequence clearly reveals that the focus initially formed in the upper right corner leads to rolls perpendicular to the subcritical wall. This solution is replaced by another one, consisting of rolls parallel to the gradient that bend in the subcritical region, better matching the requirement of being parallel to a subcritical wall.

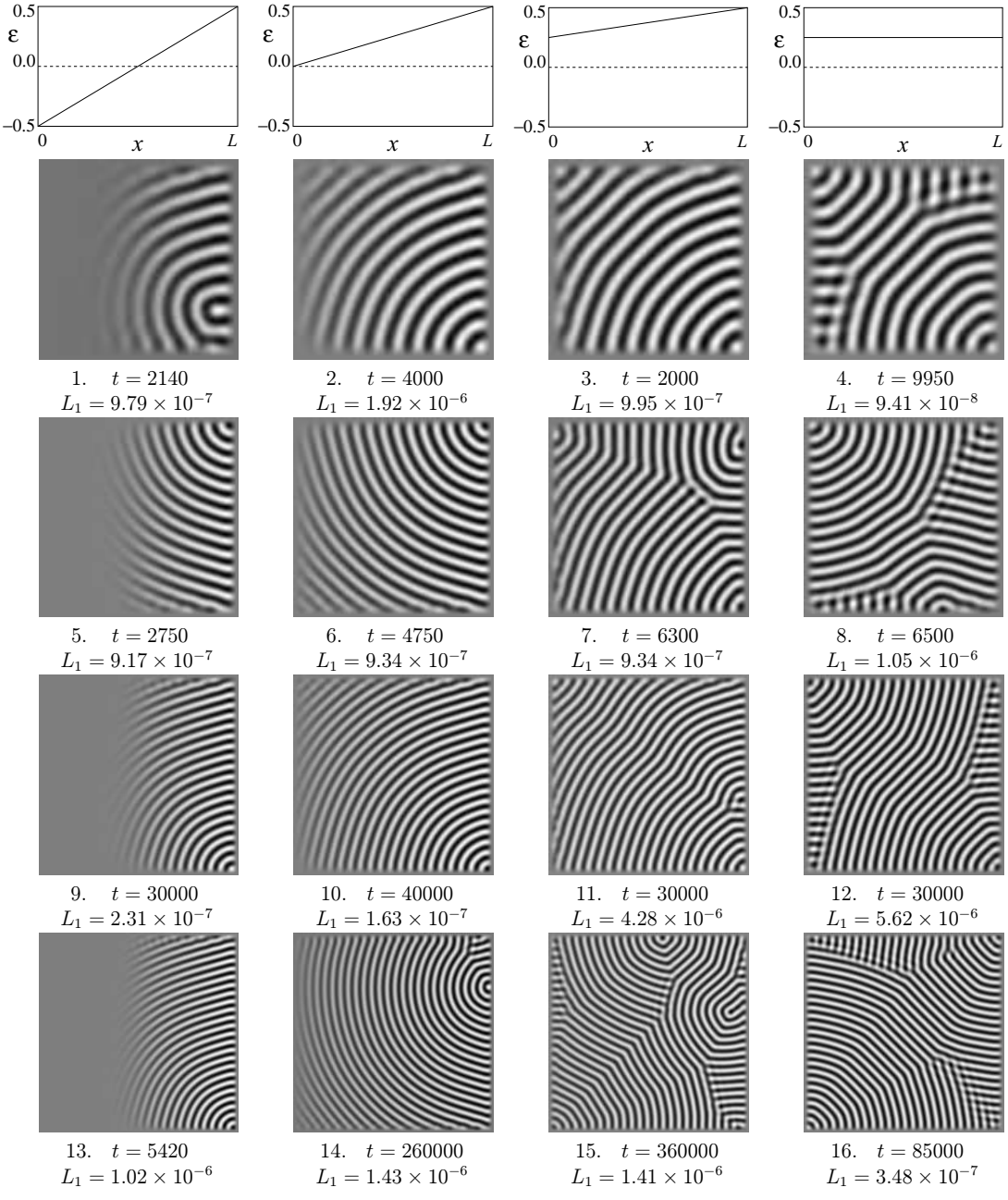

Figure 2 – Patterns obtained by integration of the Swift-Hohenberg equation in square boxes, with rigid boundary conditions, $u = \partial u/\partial n = 0$, and starting from random initial conditions. The three first columns from left to right show patterns developed in spatially ramped systems, in which the bifurcation parameter ε varies along the x-direction. Patterns in the right column refer to uniformly forced systems. The diagrams in the top of the figure show the forcing applied to the systems in each column, with the dependece of ε on x. This figure shows that uniformly forced systems submitted to a moderate forcing tend to develop patterns containing a pair of focuses located in the extremes of one of the diagonals of the box, and with rolls approching the sidewalls perpendicularly. Systems with a critical or a subcritical wall tend to develop qualitatively different patterns, with a single focus, and rolls *parallel* to that wall. This effect is clearly observed in the two first left columns. The second focus reappears when the whole system becomes supercritical, as shown by patterns in the third column from left to right. The first line of images displys patterns obtained in 20×20 boxes with grids containing 82×82 points. The second line refers to simulations performed in 30×30 boxes with grids of 122×122 points. The third line refers to 40×40 boxes and grids of 162×162 points and the last line refers to 50×50 boxes and grids of 202×202 points. All images were obtained at the end of the simulation, when the rate of evolution, L_1, presented an exponential decay.

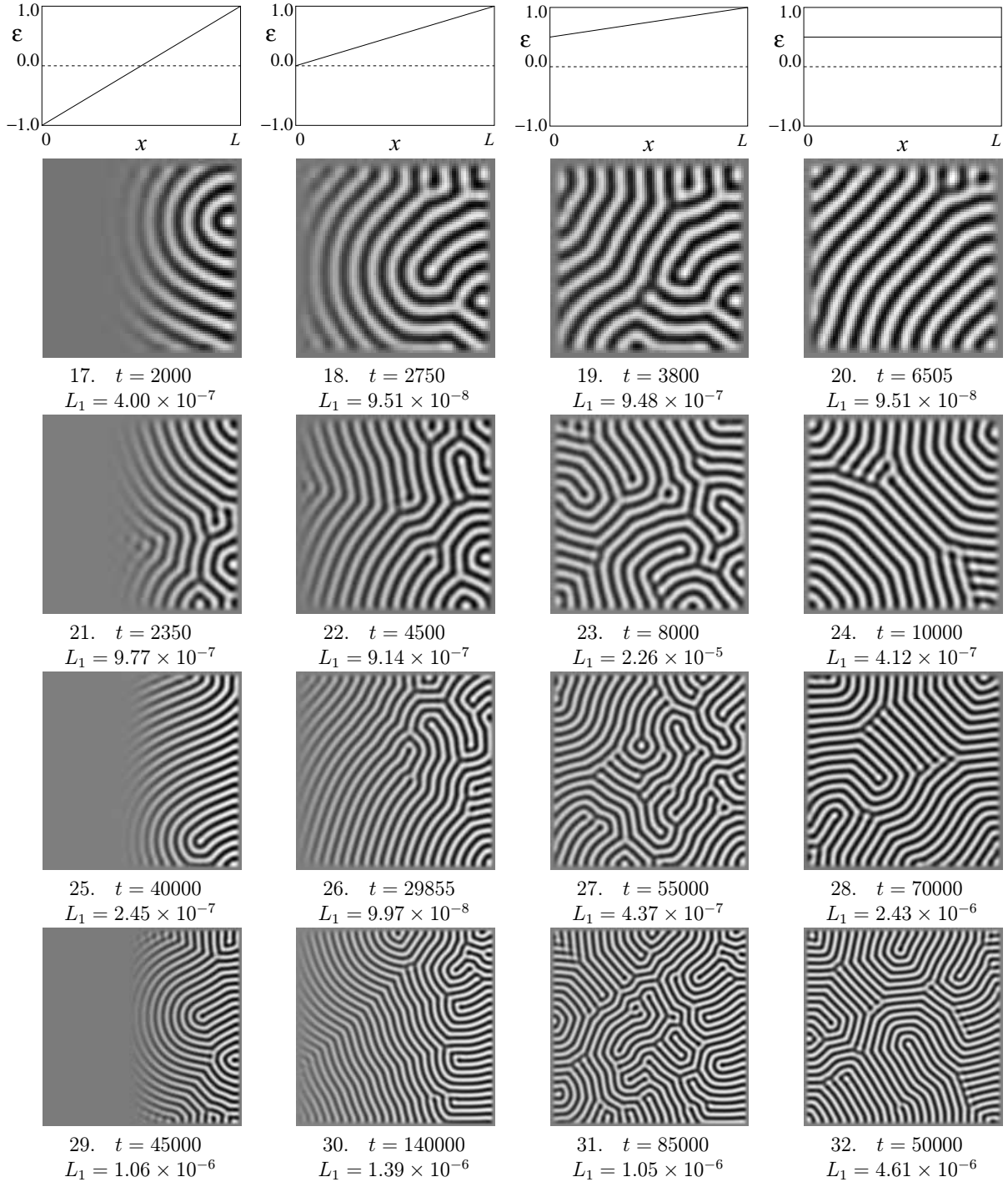

Figure 3 – Patterns obtained by integration of the Swift-Hohenberg equation under the same conditions indicated in Figure 2, except the forcing applied to the system, which is stronger than in the previous figure. The diagrams in the top of the figure show the forcing applied to the systems in each column, with the dependece of ε on x. These forcings lead to shorter coherence lengths and to patterns with higher density of defects. The tendency of uniformly forced systems to develop patterns with a pair of focuses in the extremes of one of the diagonals of the box appears less clearly than in Figure 2, particularly in the largest boxes. Nevertheless, the tendency of the rolls to become parallel to critical or subcritical sidewalls persists. All images refer to the system state at the end of the simulation, when the rate of evolution, L_1 presented an exponential decay.

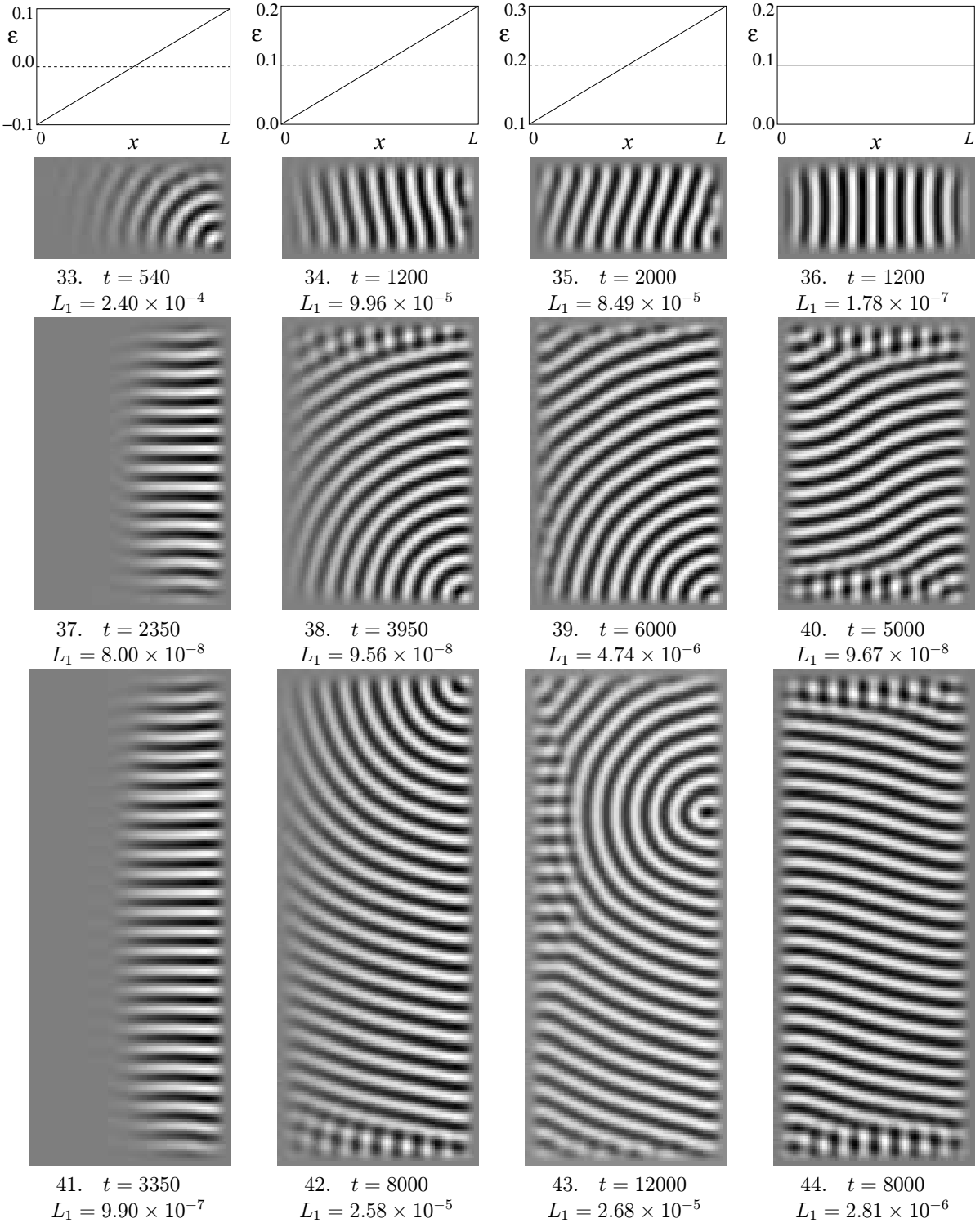

33. $t = 540$
$L_1 = 2.40 \times 10^{-4}$

34. $t = 1200$
$L_1 = 9.96 \times 10^{-5}$

35. $t = 2000$
$L_1 = 8.49 \times 10^{-5}$

36. $t = 1200$
$L_1 = 1.78 \times 10^{-7}$

37. $t = 2350$
$L_1 = 8.00 \times 10^{-8}$

38. $t = 3950$
$L_1 = 9.56 \times 10^{-8}$

39. $t = 6000$
$L_1 = 4.74 \times 10^{-6}$

40. $t = 5000$
$L_1 = 9.67 \times 10^{-8}$

41. $t = 3350$
$L_1 = 9.90 \times 10^{-7}$

42. $t = 8000$
$L_1 = 2.58 \times 10^{-5}$

43. $t = 12000$
$L_1 = 2.68 \times 10^{-5}$

44. $t = 8000$
$L_1 = 2.81 \times 10^{-6}$

Figure 4 – Patterns obtained by integration of the Swift-Hohenberg equation in 20×10, 20×30 and 20×50 boxes, with square grids containing, respectively, 82×42, 82×122, and 82×202 points. The simulations were done starting from random initial conditions and boundary conditions were assumed as $u = \partial u/\partial n = 0$. The diagrams in the top of the figure show the forcing applied to the systems in each column, with the dependece of ε with x.

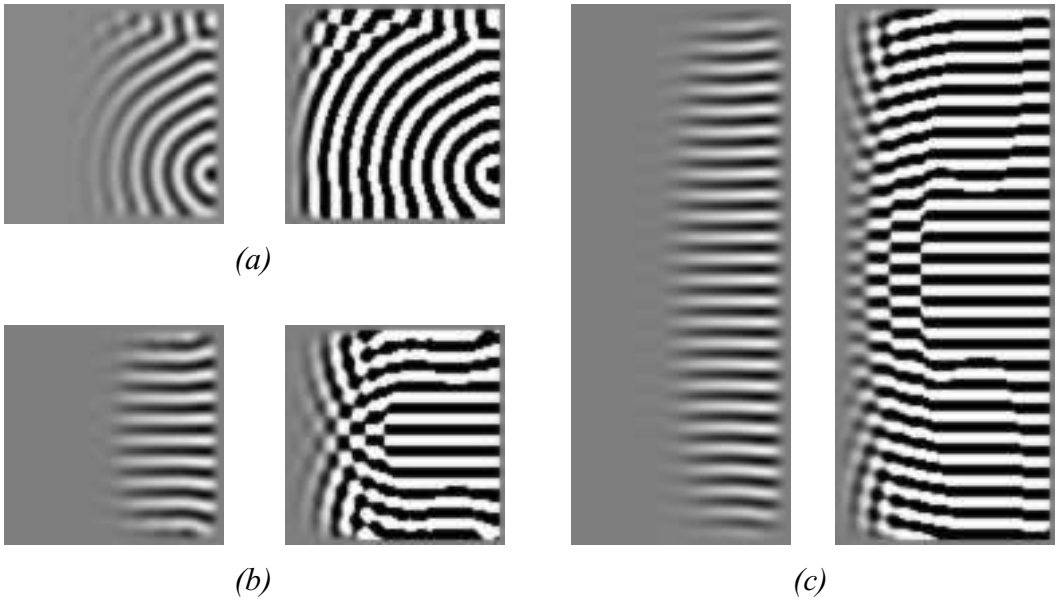

Figure 5 – The tendency of rolls to align in parallel to a subcritical sidewall. Three patterns, (a), (b) and (c), are shown with different contrasts; the left images are made with a linear scale of grays and the right ones are made with a hyperbolic tangent scale, in order to enhance the weak subcritical structure. (a): pattern obtained in a 20×20 square box forced with a ramp $-1 \leq \varepsilon \leq 1$, along the x-direction, and starting from random initial conditions. (b): pattern obtained in the same geometry, with a ramp $-0.5 \leq \varepsilon \leq 0.5$, along the x-direction, starting from initial conditions consisting a structure of rolls critical wavelength of parallel to $\mathbf{grad}\, u$. The amplitude of the initial condition is $A = 0$ for $0 \leq x \leq L/2$ and $A = \sqrt{\varepsilon/g}$ for $L/2 \leq x \leq L$.(c): pattern obtained in a a 20×50 box, forced with a ramp $-0.1 \leq \varepsilon \leq 0.1$ along the x-direction, and starting from random initial conditions. In all cases the rolls bend and tend to align in parallel to the subcritical sidewall.

4 SATURATION, PHASE DYNAMICS AND STEADY STATES

A question concerning the numerical procedure is the problem of distinguishing when we could consider a simulation as concluded. A review of the literature shows that in cases where the system evolves towards a steady state, criteria based in the saturation of the growth of the amplitude, or on the rate of change of the associated Lyapunov potential, when it exists, are often used to decide when to stop a simulation (Greenside, 1984), (Manneville, 1990). However, the evolution of a pattern results both from the effects of the saturation of the growth of the *amplitude* and from the *phase dynamics*, and these criteria are not sensitive to the evolution of the phase. The phase evolves much slower than the amplitude due, for instance, to the motion of the pattern in search of a steady state, to the dilatation or to the compression of the pattern (Eckhaus instability). In many cases, it happens that after a long and slow evolution, the process accelerates and ends by a *qualitative* change in the pattern, which we were interested in.

We followed the time evolution of patterns by monitoring the rate of change of a norm that measures the *distance* between two successive states of the system. This figure, which we call L_1 and denote by "norm", is sensitive to the evolution of both the amplitude and the phase. The norm is (Christov et al., 1995), (Pontes et al., 1995):

$$L_1 = \frac{1}{\Delta t} \frac{\sum_{i,j} \left| u_{i,j}^{n+1} - u_{i,j}^{n} \right|}{\sum_{i,j} \left| u^{n+1} \right|}, \qquad (5)$$

where the sums are made over the i and j points of the spatial grid.

An example on how this norm captures important features of the evlution of a pattern is given in Fig. 8. A focus initially formed in the right sidewall becomes unstable to a front that propagates from a new focus that appears close to the upper right corner. The phenomena is precisely refleced by the peak displayed in the $L_1 \times t$ curve.

Another example is given in Figure 9. This figure shows the time-evolution of the pattern developed in the 50×50 square, forced with a ramp $(0 \leq \varepsilon \leq 0.5)$ along the x-direction. A focus that initially penetrates from the right sidewall is forced backward. The focus disapears in $t \approx 160000$ and gives place to a new focus. The grain existing near the lower sidewall is eliminated between $t = 175000$ and $t = 180000$. After that,

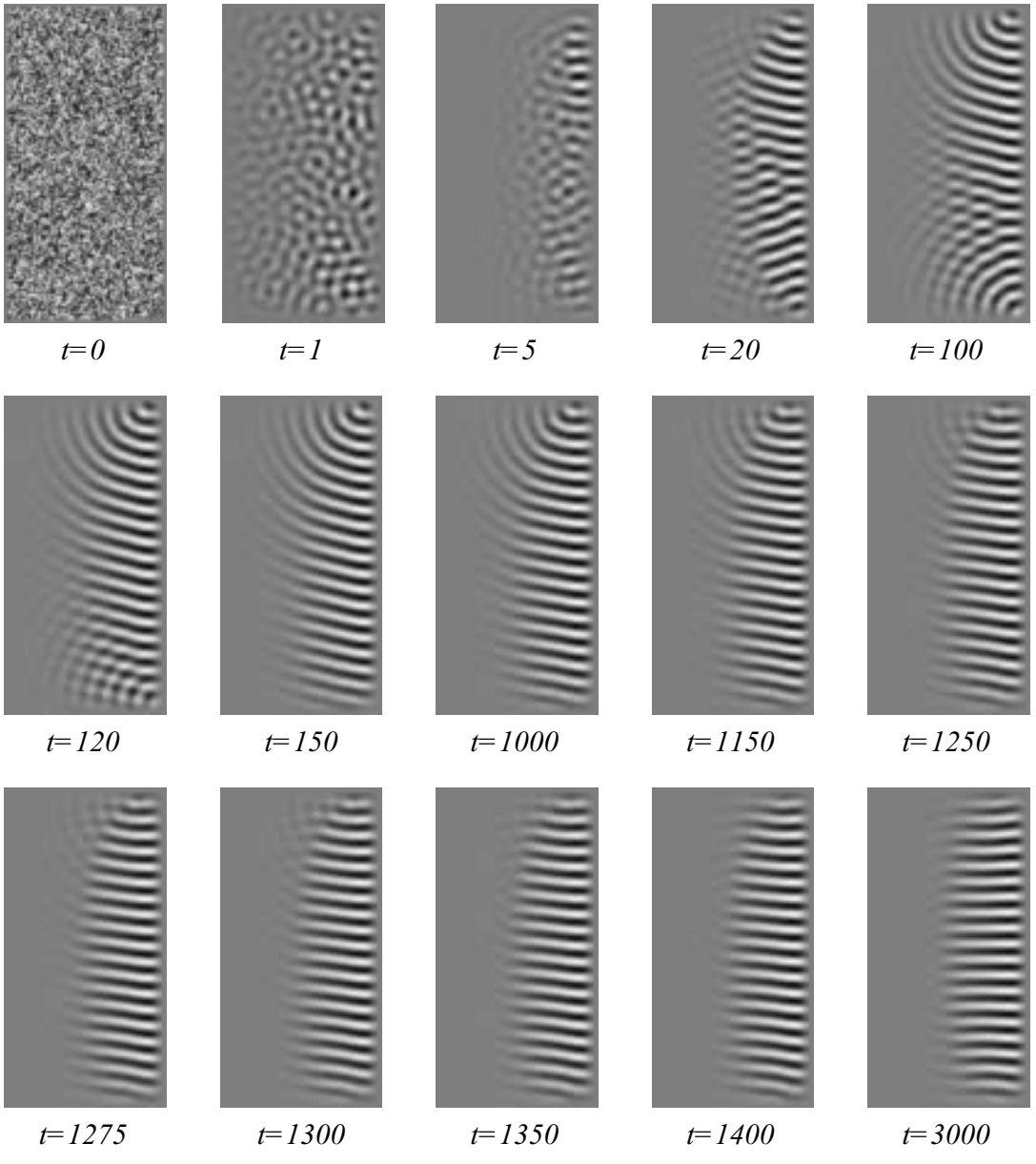

Figure 6 – Evolution of a 20×40 system, forced with a ramp $-0.1 \leq \varepsilon \leq 0.1$ along the x-direction, and starting from random initial conditions, towards a structure of rolls parallel to $\mathbf{grad}\, u$: a focus formed in the upper right corner ($t = 150$) moves to the left and finally disapears in the subcritical region, at $t \approx 150$. The final structure is parallel to the ramp (see also Fig. 7).

the system develops a small grain with rolls parallels to $\mathbf{grad}\, \varepsilon$, close to the upper right corner. The collapse of the first focus and of the grain near the lower sidewall is captured by the peaks of the $L_1 \times t$, shown in Fig. 10-II (curve b).

Figure 10 shows the $L_1 \times t$ curves associated to the evolution of patterns obtained in the 40×40 and 50×50 squares. The curves indicate that the evolution comprises a first phase characterized by a rapid decay of the norm, indicating saturation of the pattern. Several peaks are observed, associated to the elimination of defects. This phase is followed by a second one, often long, in which the norm does not exibit a sustained decay. Peaks are less frequent, or do not even appear, indicating that changes are mostly quantitative. The pattern moves slowly, i.e. the phase evolves in search of the stady state. The evolution eventually ends by a sustained exponential decay of the norm. All simulations of Eq. (1) presented this last stage, with

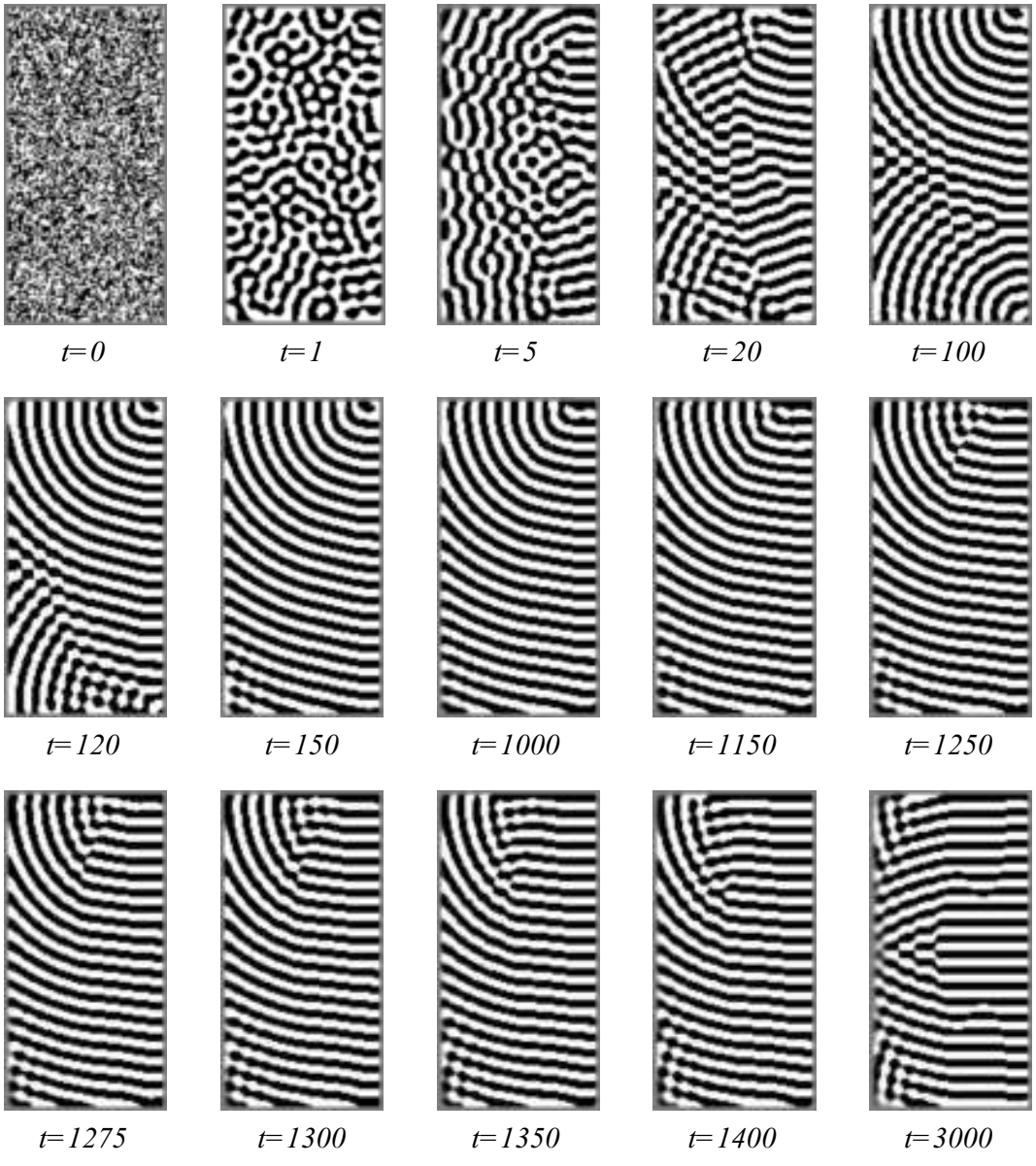

Figure 7 – Evolution of the same pattern shown in Fig. 7, with images constructed with a hyperbolic tangent scale of grays in order to enhance the subcritical structure. This figure shows that the structure aligns in parallel with the shorter sidewall due to the subcritical boundary effect, and not to the geometry or the bulk aligning effect of the ramp: the requirement of rolls parallel to the left sidewall is better fulfilled by the pattern displayed at $t = 3000$ than by the one formed at $t = 150$.

an exponential decay. At that point we stopped the integration, and considered that the system found a steady state.

5 OTHER FORCINGS AND A PATTERN CLASSIFICATION ACCORDING TO THE DENSITY OF DEFECTS

Having identified the subcritical effect responsible for rendering the rolls parallel to a subcritical wall, we asked ourselves what type of structure would the system develop if all walls were kept in subcritical conditions. In order to answer the question, we simulated a system in a 20×20 square, forced with a gaussian distribution of the bifurcation parameter, with the maximum in the center of the system, according to:

$$\varepsilon(x, y) = 0.8\, e^{-(\mathbf{r}-\mathbf{r}_0)^2/0.5} - 0.5 \qquad (6)$$

Here, the length of the square wall was set to $L = 2r$ and the coordinates of $\mathbf{r}_0$ are $(x = r,\ y = r)$. The evolution shown

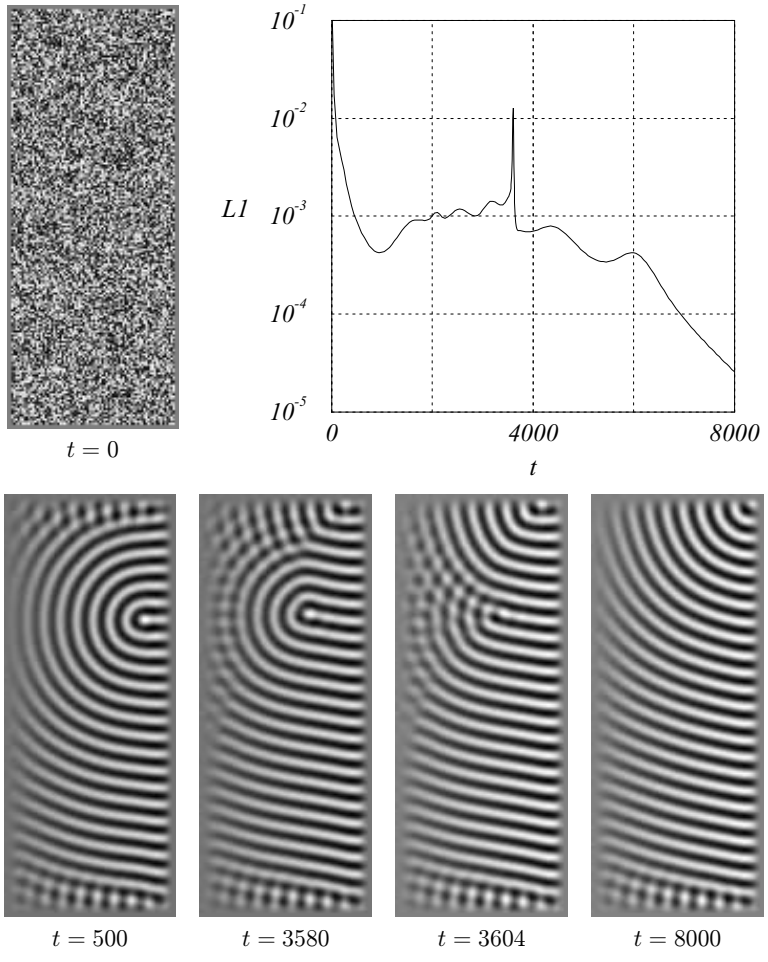

Figure 8 – The instability of a focus in a 20×50 rectangle, forced with a ramp ($0 \leq \varepsilon \leq 0.2$) along the x-direction. A focus, initially formed at the right sidewall, ($t = 500$) becomes unstable to a front that rapidly propagates in $t = \approx 3600$, from a new focus that appears close to the upper right corner. The rapid propagation of the front is precisely captured by the curve of the rate of evolution as a function of time. The simulation was performed in a grid with 82×202 points and assuming rigid boundary conditions, $u = \partial u/\partial n = 0$ at the sidewalls.

in Fig. 11 shows that the pattern initially orientates in parallel to one of the diagonals and then rotates under the influence of the subcritical effect, to become parallel to one of the walls. But if the rolls become parallel to a subcritical or slightly supercritical wall, the system does not develop a pattern parallel to all subcritical walls. The pattern effectively becomes parallel to two opposite walls but no special requirement seems to exist with respect to the other walls. Our simulations suggest that boundary subcritical effects are less restrictive than supercritical effects. Consequently, the resulting pattern exhibits a much lower density of defects than those formed in uniformly forced systems.

In fact, extended systems uniformly forced are either weakly forced and the pattern approaches the sidewalls perpendicularly, or strongly forced and this boundary requirement is no longer strictly observed. In the first case, the defects appear to match domains with different orientations defined by sidewalls. In the second case, a stronger constraint induces the melting of the structure (Walgraef 1997) by increasing of the defect density. Our results suggest that a new class of patterns, characterized by a much lower density of defects, might possibly be obtained by means of non-uniform forcings, when the boundaries are mantained at subcritical condition. Figure 12 illustrates different levels of defects obtained with the same random initial condition, but with different forcings.

6 WAVELENGTH SELECTION

An important question concerning the analysis of a pattern is the identification of the selected wavelength and of the spectral

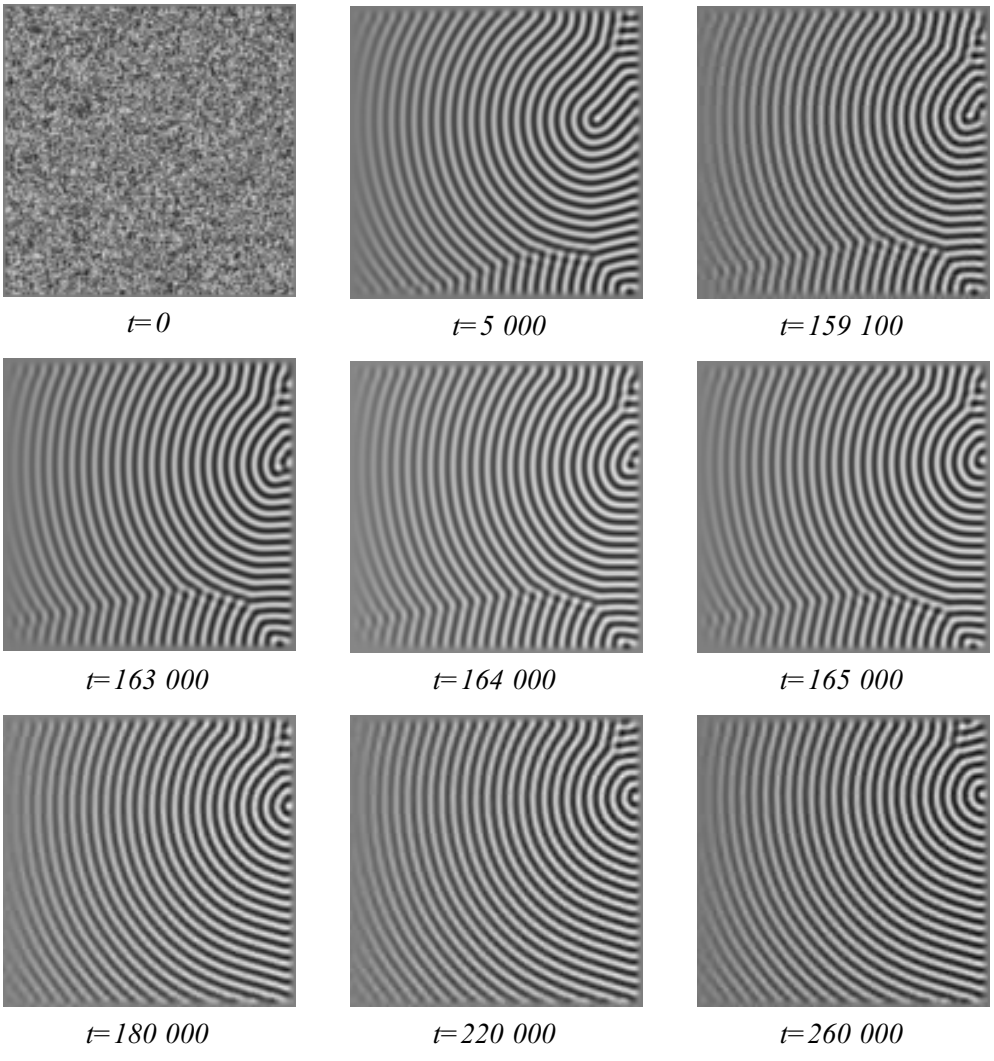

Figure 9 – The long time evolution of the pattern developed in the 50×50 square, forced with a ramp ($0 \leq \varepsilon \leq 0.5$) along the x-direction (config. # 14). A focus that initially penetrates from the right sidewall is forced backward. The focus disapears at $t \approx 160000$ and gives place to a new focus. The grain existing near the lower sidewall is eliminated between $t = 175000$ and $t = 180000$. After that, the system develops a small grain with rolls parallels to $\mathbf{grad}\,\varepsilon$, close to the upper right corner.

content of the pattern, in terms of Fourier modes. Figure 13 shows a stationary pattern and the inner part of the associated amplitude spectra of Fourier modes (b), which shows that the relevant modes fall in a cicular ring.

In order to identify the relative importance of the amplitude of the modes, irrespective of their orientation, we computed the sum of the amplitudes found in circular rings of the Fourier transform, centered at $\kappa = 0$ and limited by

$$n\Delta\kappa - \frac{\Delta\kappa}{2} \leq \kappa < n\Delta\kappa + \frac{\Delta\kappa}{2},$$

where,

$$\Delta\kappa = \frac{2\pi}{l} \quad \text{and} \quad n = 1, 2, \ldots.$$

We denote the number obtained by A. The values of A obtained accordingly were normalized by $\max(A)$ and plotted in Fig. $2(g)$, as a function of κ/κ_c.

The result is shown in Fig. $13(c)$. The curve displays an absolute maximum in $\kappa/\kappa_c = 1.04$, which we define as κ_f/κ_c, with κ_f being the *fundamental* wavenumber of the pattern. Consequently, we conclude that the fundamental *wavelength* of the pattern is, in this case, sligthly smaller than the critical wavelength. Similar results were obtained by applying the same procedure to other patterns.

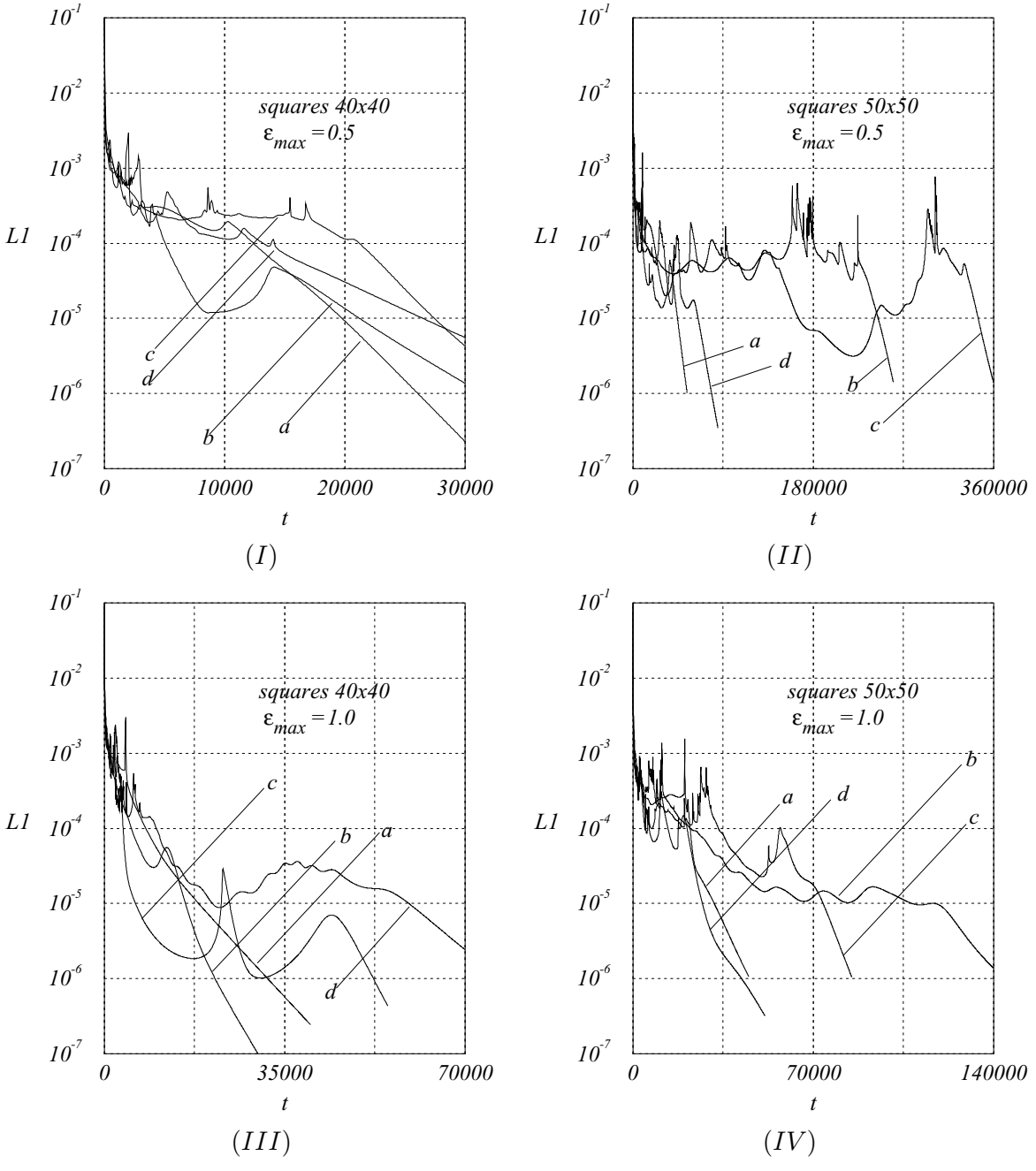

Figure 10 – The rate of evolution ($L_1 \times t$) curves associated to the 40×40 (I), and 50×50 (II) squares shown in Fig. 2 and to the 40×40 (III), and 50×50 (IV) squares shown in Fig. 3. The curves labelled a, b and c refer to systems forced with a ramp of ε and d, to uniformly forced systems. Curves identified by a refer to ramped systems in which the critical point is located in $x = L/2$, b in $x = 0$, c in $x = -L$ and d, to uniformly forced systems. L is the length of the sidewall. These curves show that system evolution comprises three stages: In the first one, the L_1 norm rapidly decays and displays sharp peaks, in the second stage, the *phase* of the pattern evolves and in the last one the rate of evolution presents an exponential decay.

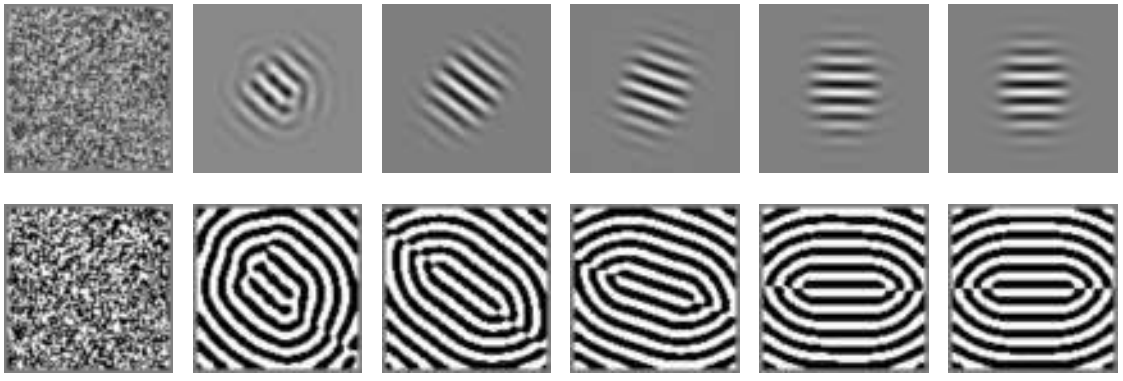

Figure 11 – Evolution of a pattern in 20×20 system, forced with a gaussian distribution of the bifurcation parameter, according to $\varepsilon(x, y) = 0.8\exp(-2(\mathbf{r} - r_0)^2) - 0.5$. The length of each sidewall is $L = 2r$ and the cordinates of $\mathbf{r}_0$ are $x = r$ and $y = r$. The numerical grid contains 82×82 points. The tendency of the rolls to align with the subcritical sidewalls appears again in this case.

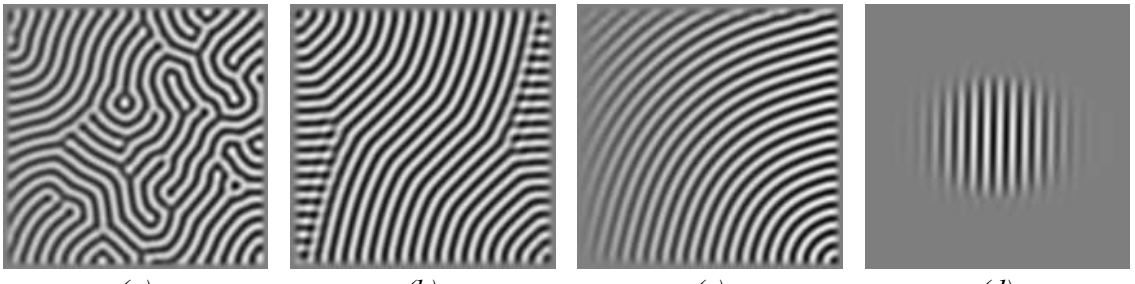

Figure 12 – Four levels of defects in 40×40 systems. (a): system forced with a ramp $0.5 \leq \varepsilon \leq 1$, along the x-direction. The strong forcing leads to a high density of defects. (b): system moderately and uniformly forced ($\varepsilon = 0.25$), displaying a pattern characterized by a pair of focuses in the extremes of a diagonal. (c): moderately forced system, with a ramp $0. \leq \varepsilon \leq 0.5$, along the x-direction. The pattern contains a single focus. (d): on-uniformly forced system, with *all* boundaries in subcritical conditions; the boundary effects, which are less restrictive than with supercritical sidewalls, lead to the lowest density of defects. All patterns were obtained from the same random initial condition.

7 COMPARISON TO OTHER WORKS

Our numerical work includes the simulation of uniformly forced systems, conducted with the twofold purpose of identifying differences with respect to patterns formed in ramped systems, and comparing the results with existing data, in particular with those found in the classical paper of Greenside and Coughram Jr. (1984). The model equations integrated in this work and by the above authors are:

$$0.0509\,\frac{\partial u}{\partial t} = \varepsilon u - 1.29\,u^3 - 0.015\left(\nabla^2 + 3.1172^2\right)^2 u$$

(This work)

$$\frac{\partial u}{\partial t} = \varepsilon u - u^3 - \left(\nabla^2 + 1\right)^2 u$$

(Greenside and Coughram Jr.)

A comparison of our results to those obtained by Greenside and Coughram Jr. reveals good qualitative agreement between the patterns obtained in both works. In one particular case the system dimensions and the forcing adopted are pratically the same, allowing a direct comparison of the quantitative results, as shown in Table 2. May we stress the differences in the parameters adopted in the two works: our simulations were performed with a grid of aproximately 8 points per wavelength, whereas these authors adopted 12 points per wavelength; the random initial conditions are different; furthermore, we adopted a smaller coefficient in the term containing the space derivatives, that results in shorter coherence lengths; to conclude, the criteria used to identify steady states are different: these authors used the rate of change of the associated Lyapunov potential and we used the L_1 norm, which is more restrictive. The differences in the aspect ratio and in the

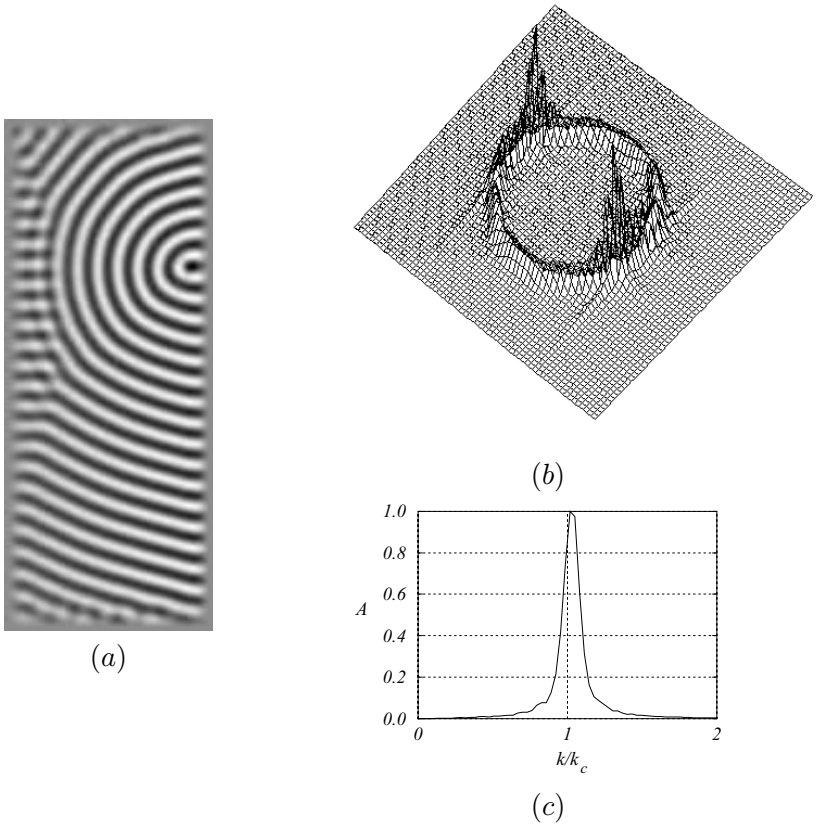

Figure 13 – The spectral content of the pattern (a), displayed in a 20×50 box, forced with a ramp $0 \leq \varepsilon \leq 0.2$, along the x-direction. (b) the Fourier transform of the pattern shown in (a). (c): wavenumbers existing in the pattern. A is the summ of amplitudes in all directions, associated to wavenumbers comprised between κ and $\kappa + \Delta\kappa$, where $\Delta\kappa$ is the mesh of the discrete Fourier transform. This number is plotted as a function of κ/κ_c. The peak, located in $\kappa/\kappa_c = 1.04$ defines the fundamental mode of the pattern, κ_f, which is slightly larger than the critical.

Table 2 – Comparison between data and results concerning one of the simulations presented herein (20×30 rectangle forced with $\varepsilon = 0.1$) and a similar simulation performed by Greenside and Coughram Jr. (1984). L_x and L_y are the system length and width, expressed in number of critical rolls; F is the ratio between the geometric aspect ratio of the box and the *coherence length* of the pattern (Eq. 4); n_x and n_y are the number of points of the spatial grid along the x and the y directions; *mesh* is the approximate number of points per wavelength of the grid adopted in the simulations.

	L_x	L_y	ε	F	t_s	t_s/τ_0	n_x	n_y	*mesh*
This work (config. # 40)	29.8	19.8	0.1	27.1	5000	98232	122	82	8
Greenside and Coughram Jr.	29.2	19.5	0.1	9.2	12640	12640	193	128	12

criteria adopted to conclude a simulation explain the relaxation time t_s/τ_0 obtained in our simulation, which is almost 8 times higher than the value presented by these authors.

To our knowledge no results have been published concerning numerical simulations of the ramped Swift-Hohenberg model. Common points with the theoretical work of Walton (1983) and Dewel et al. (1993), and with the experimental work of Srulijes (1979) have already been discussed above.

8 THE SWIFT-HOHENBERG MODEL WITH QUADRATIC TERMS

It can be shown that the amplitude equations of a hexagonal structure developed in spatially ramped Rayleigh-Bénard convection include quadratic convective-like terms, and this result suggests that a modification could be made in the Swift-Hohenberg model to include similar terms. Based on that we performed some

numerical simulations of the model, in the form:

$$\tau_0 \frac{\partial u}{\partial t} = \varepsilon u + \nu u \left(\frac{\partial u}{\partial x} + \frac{\partial u}{\partial y} \right) - g u^3 - \xi^4 \left(\nabla^2 + k_0^2 \right)^2 u$$

The boundary conditions and the numerical values adopted for the coefficients are the same as previously used. We considered ramped systems with $0 \leq \varepsilon \leq 0.5$ along the x direction and uniform forcing, with $\varepsilon = 0.25$. The coefficient ν was set to 1.5, 2.2, 2.5, 3.5 and 5.0. The results are summarized in Fig. 14. At $\nu = 1.5$ and uniform forcing we obtained a stationary pattern of straight rolls, parallel to one diagonal. By forcing the system with a ramp of ε, stationary patterns were no longer obtained: at low values of ν rolls move in the sense opposite to $\mathbf{grad}\,\varepsilon$. The norm L_1 displays a periodic behaviour. By increasing ν the pattern undergoes a transition to a structure of squares and the norm is longer periodic. Finally, the whole structure becomes chaotic.

9 THE SWIFT-HOHENBERG MODEL WITH A NONPOTENTIAL CUBIC TERM

In the previous section we reported the results of our simulations of the Swift-Hohenberg equation including a convective-like term, suggested by the existence of this kind of term in the amplitude equations of a structure containing three modes forming, successively, an angle of $2\pi/3$. Other modifications of the Swift-Hohenberg equation have also been used to study Rayleigh-Bénard convection. Manneville (1990) adopted a cubic nonlinear term in the form $-\left(u^2 + (\nabla u)^2\right) u$ and Greenside and Coughran Jr. (1984) investigated pattern formation using the cubic term in the form $-(\nabla u)^2 u$. In both cases the resulting patterns evolved towards stationary patterns. Cross et al. (1886) considered a variation of the Swift-Hohenberg equation in the following non-variational form:

$$\tau_0 \frac{\partial u}{\partial t} = \varepsilon u + 3 \left| \nabla u \right|^2 \nabla^2 u - \xi^4 \left(\nabla^2 + \kappa_0^2 \right)^2 u, \quad (7)$$

with $\kappa_0 = \tau_0 = \xi = 1$. These authors focused on the problem of wavenumber selection, and considered several pattern configurations in rectangular and in circular containers. They reported wavelenghts smaller than the critical one, and decreasing as the control parameter ε increases. Nevertheless, the selected wavelength was found to depend on the type of pattern developed. The authors concluded that no general wavenumber selection principle exists in the framework of Eq. (7).

In addition, Cross et al. found a periodic time-dependent pattern, where they observed a translation of the rolls. In this section we present the results concerning a numerical simulation of Eq. (7) in a 40×40 box, forced with a ramp of the bifurcation parameter $-0.5 \leq \varepsilon \leq 0.5$ along the x-direction. The parameters were set to $\kappa_0 = 3.1172$ and $\tau_0 = 0.0509$ as before, and the simulation was performed using a time step $\Delta t = 0.05$. The results, summarized in Fig. 15, essentially comply with our findings obtained by simulation of the Swift-Hohenberg equation in ramped systems. The system develops a structure containing a single focus in the sidewall where the bifurcation parameter attains the maximum. The rolls tend to orientate in parallel with the most subcritical sidewall, in the neighbourhood of that wall. In other words, one of the main findings presented in this work, the boundary subcritical effect, also appears upon modelling Rayleigh-Bénard convection with Eq. (7). The state of the system at the end of the simulation ($t = 15000$) is shown in Fig. 15a. The curve of the velocity of evolution, $L_1 \times t$, shown in Fig. 15b, captures the periodic time-dependent nature of the asymptotic state. The period is $T = 450$. The Fourier transform of the pattern shows that the relevant modes do not fall exactly in a circular ring with average radius equal to the critical one, but in a more irregular figure. In order to characterize the selected wavelength of the structure we plotted, as before, the sum of the amplitudes of the modes located in rings with thickness $\Delta\kappa$ against κ/κ_c. The curve displays a maximum in $\kappa/\kappa_c =$, defining the fundamental mode of the pattern, $\kappa_f = 1.06\kappa_c$. Again in this case, the selected wavelength is slightly bigger than the critical one.

10 CONCLUSIONS

This work addresses the problem of pattern formation in extended Rayleigh-Bénard systems submitted to a spatial non-uniform forcing. The analysis was performed by numerical integration of the Swift-Hohenberg equation, in systems confined by rigid sidewealls. There are two main results: first, the bulk orientation effect of the gradient is always dominated by boundary effects in our simulations. Second, we identified a clear boundary subcritical effect requesting rolls to be parallel to a subcritical wall. The effect is strong enough to qualitatively change a pattern with respect to those obtained under uniform forcing: rolls parallel to a wall are automatically perpendicular to adjacent walls and a focus is no longer required, as in uniformly forced systems. Typically, the latter display a pair of focuses in the extreme of a diagonal, whereas ramped systems with a critical or subcritical wall develop patterns with a single focus. The effect suggests that non-uniform forcing might provide means to control the density of defects in systems displaying a roll pattern. Simulations in which all boundaries were

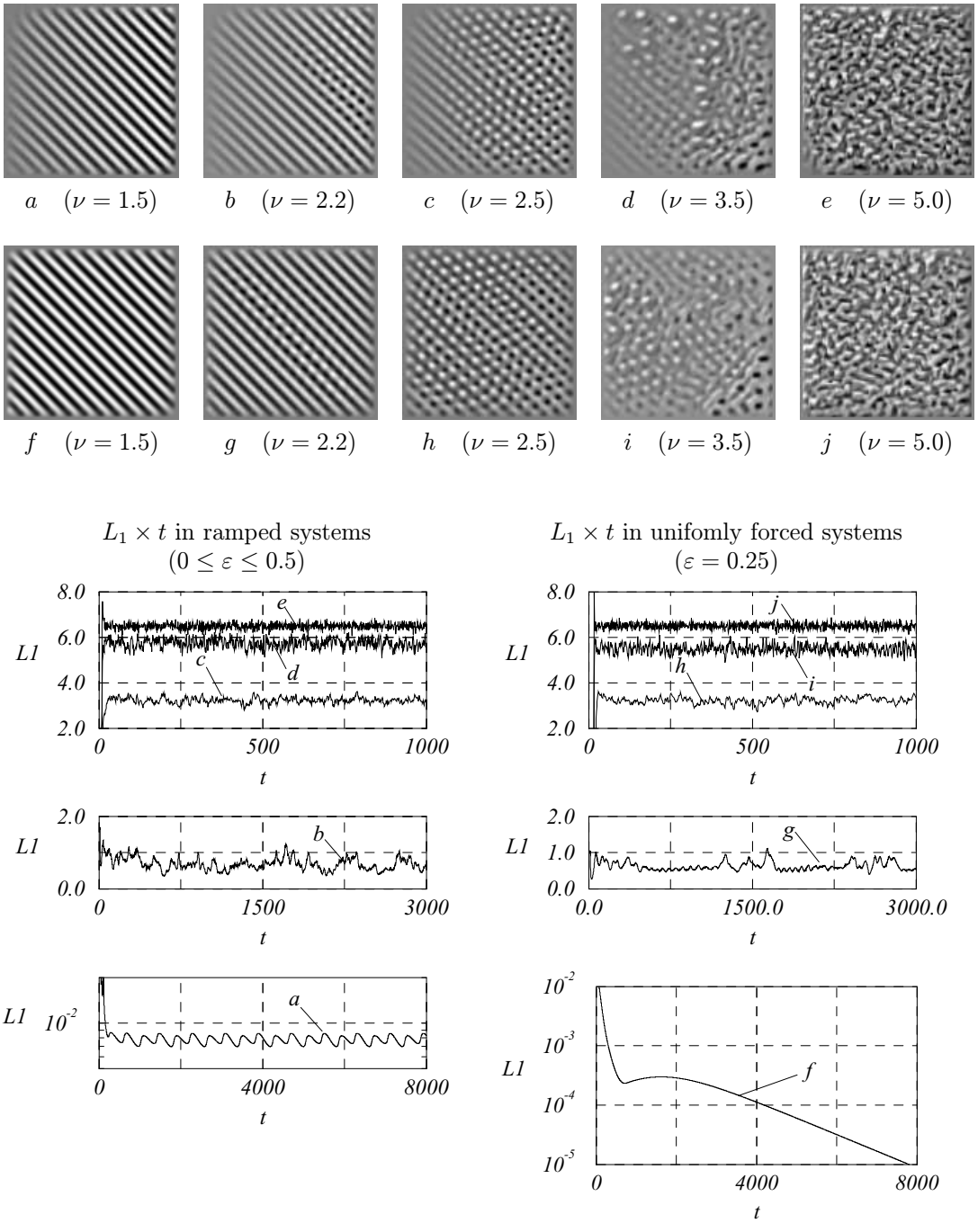

Figure 14 – Simulation of the Swift-Hohenberg equation including a convective-like term in the form $\nu(\partial u/\partial x + \partial u/\partial y)$, in a 30×30 system, using grids with 122×122 points. The first line of images refers to systems forced with a ramp $0 \leq \varepsilon \leq 0.5$, along the x-direction. The second line of images refers to uniformly forced systems, with $\varepsilon = 0.25$. The associated $L_1 \times t$ curves show that uniformly forced systems, in which the coefficient ν of the quadratic terms is sufficiently small, evolve to a steady pattern (f). Ramped systems display a periodic time-dependent behaviour, even for low values of ν (a). Upon increasing this coefficient, the system evolves to aperiodic time-dependent behaviours.

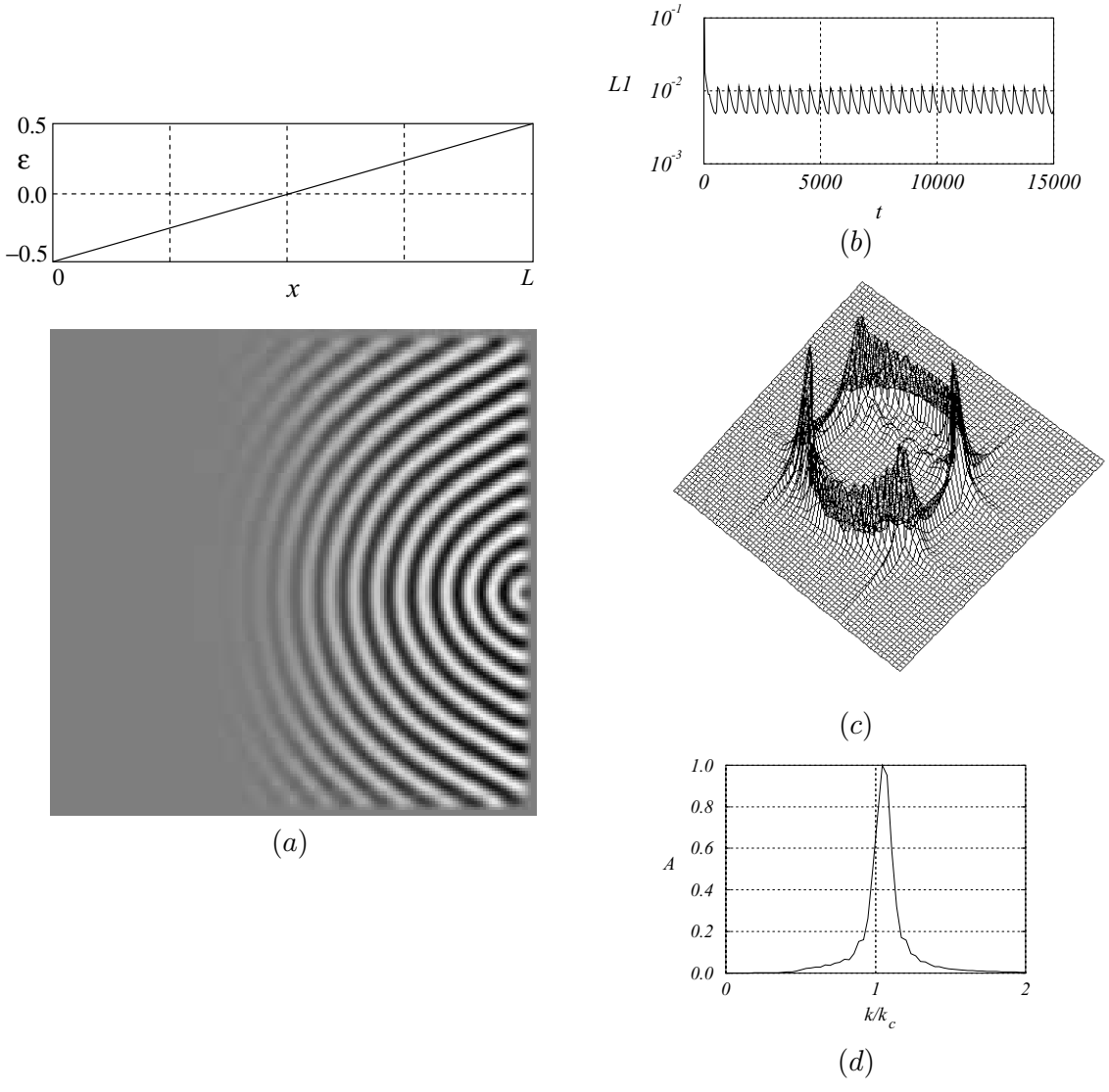

Figure 15 – Results concerning a simulation of the Swift-Hohenberg equation with the cubic term in the form $3\,|\nabla u|^2\,\nabla^2 u$. (a) shows the system state at $t = 15000$ and the diagram with the distribution of the bifurcation parameter along the x-direction. (b): the curve of the rate of evolution of the pattern, $L_1 \times t$, which shows that the system presents a periodic time-dependent behaviour. (c): the Fourier transform of the pattern shown in (a). (d): wavenumbers existing in the pattern. The peak, located in $\kappa/\kappa_c = 1.06$ defines the fundamental mode, κ_f, which is larger than the critical and slightly larger than the fundamental mode identified in the simulations performed with the cubic term in the form $g\,u^3$.

mantained in subcritical conditions developed patterns totally free of defects in the supercritical region. We also performed simulations of non-potential versions of the Swift-Hohenberg equation. In all cases, the local wavelength of the patterns remain close to the critical one.

The time evolution of the patterns was followed by monitoring the velocity of evolution of a norm measuring the distance between two successive states of the system. This measure, contrary to those based on saturation on the rate of change of the associated potential, also captures the phase evolution. This evolution is much slower than the saturation process, but far from monotonous. In some cases, it ended with a collapse of a defect and a qualitative change of the pattern. In all cases we observed a final exponential decay of the rate of evolution of the norm, showing that the system approaches a steady state.

Hence, it clearly appears in our analysis that the system behaviour is dominated by boundary effects, irrespectively of its size, when the ramp defines a super and a subcritical region

in the convection cell. This may be related to the fact that the system passes through criticality somewhere in the domain, where the correlation length diverges. In this case, the usual separation into bulk and boundary domains is meaningless, even in extended systems. To conclude, we think that our numerical results suggest that further theoretical and experimental investigations are needed to reach a better understanding of subcritical boundary effects and of the interaction between super and subcritical domains in extended systems.

ACKNOWLEDGMENTS

J.P. acknowledges the support of a doctoral fellowship (202092-89.5/EM) from the Brazilian National Council for Scientific and Technological Development, CNPq, the continuous support from Promon Engenharia Ltda. (Brazil), and a post-doctoral fellowship from the Spanish Ministry of Education and Science. He also acknowledges the interest of profs. G. Nicolis and the hospitality of the Free University of Brussels, where most of this work was done. This work was also supported by the EU grant CI 1*–CT 92–0006.

A THE NUMERICAL METHOD

The Swift-Hohenberg equation was solved by means of a finite difference method using a semi-implicit splitting-type scheme. The scheme is detailed in a paper by Christov et al. (1997). For the sake of completenss we sketch here the main features of the scheme.

Creating effective numerical schemes and algorithms for diffusion equations and their generalizations vindicates considerable effort due to important applications of these models. A variety of different schemes has been created for the equation with second-order diffusion (heat-conduction equation). The time stepping of the solution can be done either by spectral (see the illuminating work Frati et al. (1992)) or by explicit or implicit schemes with finite differences or finite elements, or by certain combination of these. In Ekebjaerg and Justtesen (1991), an explicit scheme allowing vectorization is proposed for the advection-diffusion equation. The condition of stability of an explicit scheme imposes, as a rule, very restrictive limitations on the time increment. It is much more realistic for the fourth-order derivatives when $\Delta t \leq \frac{1}{4}h^4$. This is an evidence why the problem of constructing implicit schemes is of significance. However, the straightforward implementation of an implicit scheme in more than one spatial dimensions results into very large linear systems whose solution are not easily tenable on desktop computer platforms.

An effective way to combine the stability properties of implicit schemes and the cost-efficiency of the explicit ones is to use the so-called coordinate splitting. The time step is implemented through several half-time steps in which only one of the operators is implemented implicitly. The notion of splitting was introduced in Peaceman and Rachford (1955), Douglass and Rachford (1956) for the second-order parabolic equation (heat equation) and proved very fruitful (see Yanenko (1971) for review of the earlier results).

The coordinate splitting method is still one of the most popular techniques for solving advection-diffusion problems. In Mampaey (1990) is developed an Alternating Directions Implicit (ADI) scheme for studying solidification problems where special care is needed since the temperature oscillations in the interface between the phases may cause instability. In Hewett et al. (1992) is applied the so-called "dynamic" ADI to strongly coupled second-order equations and it is shown that the splitting method requires one order less of magnitude for storage and it is one order of magnitude faster. The coordinate splitting requires special approach in case of complex domains. The problems connected with applying ADI together with domain composition are treated in Rosenfeld and Yassour (1994) where numerical solution is obtained for variety of complex-shaped domains. A new class of time-stepping algorithms is developed in Armero and Simo (1992) for strongly coupled thermomechanical problems.

The original PDE is replaced by the following form, with a first order discrete representation of the time derivative:

$$\begin{aligned}\tau_0 \frac{u^{n+1}-u^n}{\Delta t} &= \varepsilon(x)\,u^n - 3g\,(u^n)^2 u^{n+1} + 2g\,(u^n)^3 \\ &\quad - \xi^4\left(\frac{\partial^4}{\partial x^4} + \frac{\partial^4}{\partial y^4} + \kappa_0^4\right) u^{n+1} \\ &\quad - 2\,\xi^4 \frac{\partial^4 u^n}{\partial x^2 \partial y^2} \\ &\quad - 2\,\xi^4 \kappa_0^2 \left(\frac{\partial^2}{\partial x^2} + \frac{\partial^2}{\partial y^2} +\right) u^n,\end{aligned} \tag{8}$$

where u^n and u^{n+1} denote the dependent variable evaluated in the time steps n and $n+1$, respectively. Upon defining the operators Λ_x^n, Λ_y^n, and the function f^n, by:

$$\Lambda_x^n = -\xi^4 \frac{\partial^4}{\partial x^4} - \xi^4 \frac{\kappa_0^4}{2} - \frac{3}{2} g\,(u^n)^2$$

$$\Lambda_y^n = -\xi^4 \frac{\partial^4}{\partial y^4} - \xi^4 \frac{\kappa_0^4}{2} - \frac{3}{2} g\,(u^n)^2$$

$$f^n = \varepsilon(x)\,u^n + 2g\,(u^n)^3 - 2\,\xi^4 \frac{\partial^4 u^n}{\partial x^2 \partial y^2} - 2\,\xi^4 \kappa_0^2\,\nabla^2 u^n,$$

we may write equation (8) in the form:

$$\frac{u^{n+1} - u^n}{\Delta t} = \left(\Lambda_x^n + \Lambda_y^n\right) u^{n+1} + f^n, \qquad (9)$$

or:

$$\left(I - \left(\Lambda_x^n + \Lambda_y^n\right)\right) u^{n+1} = \Delta t \left(u^n + f^n\right). \qquad (10)$$

Here I is the identity operator. The inversion of the operator

$$\left(I - \left(\Lambda_x^n + \Lambda_y^n\right)\right)$$

requires a considerable computational effort, since the unknowns are coupled with those lying both in the neighbouring lines *and* columns, through the spatial derivatives in two directions. For this reason we used the *stabilizing correction scheme*, through which Eq. (10) is splitted in the following two (Christov and Ridha 1994) and (Christov et al. 1995):

$$\left(I - \Delta t\,\Lambda_x^n\right)\tilde{u} = \left(I + \Delta t\,\Lambda_y^n\right) u^n + \Delta t\,f^n, \qquad (11)$$

$$\left(I - \Delta t\,\Lambda_y^n\right) u^{n+1} = \tilde{u} - \Delta t\,\Lambda_y^n\,u^n. \qquad (12)$$

To prove that Eqs. (11-12) are equivalent to (9) it suffices to apply the operator $\left(I - \Delta t\,\Lambda_x^n\right)$ to Eq. (12) and add the result to Eq. (11). We get:

$$\left(I + (\Delta t)^2 \Lambda_x^n \Lambda_y^n\right) \frac{u^{n+1} - u^n}{\Delta t} = \left(\Lambda_x^n + \Lambda_y^n\right) u^{n+1} + f^n,$$

hence the splitting scheme is equivalent to Eq. (9), within a second order correction. The advantage of the splitting is twofold: The operator in the left hand side of Eqs. (11) and (12) displays a penta-diagonal structure, when the space operators approximated to second order, on the difference level. The elements of these operators are just numbers and not matrices, as in the case of Eq. (10). Second, Eq. (11) can be solved line by line and Eq. (12) can be solved column by column, reducing considerably the storage requirements. The penta-diagonal systems were then solved by Gaussian elimination (Christov 1994).

This numerical scheme generalizes to the case of fourth-order diffusion operators, the classical coordinate splitting introduced by Peaceman and Rachford (1955), Douglass (1956) and Yanenko (1971).

The scheme proved to be stable with *all* time-steps used in the tests conducted to qualify our numerical code. Nevertheless, beyond a certain limit, an increase in the time-step results in an increase in the time required by the system to attain a given state, suggesting that there exists an *optimum* time-step, which minimizes the number of steps accomplished in each run. In most of our simulations we attempted to use that optimum time-step, which we found to be $\Delta t = 0.05$. May we mention that this optimum time-step scales with the value adopted for the coefficient τ_0 of the Swift-Hohenberg equation, which we set to $\tau_0 = 0.0509$. Consequently, in the case where $\tau_0 = 1$, we expect an optimum time-step $\Delta t \approx 1$. The largest simulations performed in this work were run in grids with 202×202.

In the simulations performed with the quadratic convective-like term, we adopted a similar numerical scheme, and assigned that term to the "old" time-step. In the simulations performed with the cubic term in the form $3\,|\nabla u|^2\,\nabla^2 u$, we adopted the following scheme:

$$\tau_0 \frac{u^{n+1} - u^n}{\Delta t} = \varepsilon(x)\,u^n + 3\,|\nabla u^n|^2\,\nabla^2 u^{n+1} - \xi^4 \left(\frac{\partial^4}{\partial x^4} + \frac{\partial^4}{\partial y^4} + \kappa_0^4\right) u^{n+1} - 2\,\xi^4 \frac{\partial^4 u^n}{\partial x^2 \partial y^2} - 2\,\xi^4 \kappa_0^2\,\nabla^2 u^n. \qquad (13)$$

The operators Λ_x^n, Λ_y^n, and the function f^n are, in this case defined by:

$$\Lambda_x^n = -\xi^4 \frac{\partial^4}{\partial x^4} - \xi^4 \frac{\kappa_0^4}{2} + 3\left|\nabla u^n\right|^2 \frac{\partial^2}{\partial x^2}$$

$$\Lambda_y^n = -\xi^4 \frac{\partial^4}{\partial y^4} - \xi^4 \frac{\kappa_0^4}{2} + 3\left|\nabla u^n\right|^2 \frac{\partial^2}{\partial y^2}$$

$$f^n = \varepsilon(x)\,u^n - 2\,\xi^4 \frac{\partial^4 u^n}{\partial x^2 \partial y^2} - 2\,\xi^4 \kappa_0^2\,\nabla^2 u^n,$$

The splitting of Eq. (13) in two, was made as in the preceeding case.

REFERENCES

ARMERO F & SIMO JC. 1992. A new unconditionaly stable fractional step method for nonlinear coupled thermo-mechanical problems. Int. J. Num. Meth Engn., 45: 737.

BRAGARD J, PONTES J & VELARDE MG. 1996. Patterns, defects and evolution of Bénard-Marangoni cells. Int. J. Bifurcation and Chaos, 6(9): 1665–1671.

BROWN SN & STEWARSON K. 1977. On thermal convection in a large box. SIAM, 57: 187–204.

CHANDRASEKHAR S. 1961. Hydrodynamic and Hydromagnetic Stability. Dover, New York.

CHRISTOV CI. 1994. Gaussian elimination with pivoting for multidiagonal systems. University of Reading.

CHRISTOV CI & RIDHA A. 1994. Splitting scheme for iterative solution of bi-harmonic equation. In: I. DIMOV et al. (Ed.), Adv. in Num. Meth. and Appl., pages 341–352. World Scient.

CHRISTOV CI, PONTES J, WALGRAEF D & VELARDE MG. 1997. Implicit time splitting for fourth-order parabolic equations. Comput. Methods Apll. Mech. Engrg., 148: 209–224.

CROSS MC. 1982. Boundary conditions on the envelope functions of convective rolls close to the onset. Phys. Fluids, 25: 936–941.

CROSS MC. 1982. Ingredients of a theory of convective textures close to onset. Phys. Rev. A, 25: 1065–1076.

CROSS MC, TESAURO G & GREENSIDE HS. 1986. Waveneumber selection and persistent dynamics in models of convection. Physica D, 10: 12–18.

DE WIT A. 1993. Brisure de symétrie spatiale et dynamique spatiotemporalle dans les systèmes réaction-diffusion. PhD thesis, Université Libre de Bruxelles, Brussels.

DEWEL G & BORCKMANS P. 1989. Effects of slow spatial variations on dissipative structures. Phys. Lett. A, 138: 189–192.

DOUGLASS J & RACHFORD HH. 1956. On the numerical solution of heat conduction problems in two and three space variables. Trans. Amer. Math. Soc., 82: 421–439.

EKEBJAERG L & JUSTTESEN P. 1991. An explicit scheme for advection-diffusion modelling in two-dimensions. Comp. Meth. Appl. Mech. Engineering., 88: 287–297.

FRATI A, PASQUARELLY & QUARTERONI A. 1992. Spectral Approximation to advection-diffusion problems by fictious interfce method. J. Comput. Physics., 107: 201–212.

GREENSIDE HS and COUGHRAM Jr WM. 1984. Non-linear pattern formation near the onset of Rayleigh-Bénard convection. Phys. Rev. A, 30: 398–428.

HEWETT DW, LARSON DJ & DOSS S. 1992. Solution of simultaneous partial differential equations using dynamic ADI: Solution of streamlined darwin field equation. J. Comp. Phys., 101: 11–24.

HOYLE RB. 1995. Steady squares and hexagons on a subcritical ramp. Phys. Rev. E, 51: 310–315.

KELLY RE & PALL D. 1976. Thermal convection induced between nonuniformly heated horizontal surfaces. In: Proceedings of the 1976 Heat Transfer and Fluid Mechanics Institute, pages 1–17. Stanford U.P.

KIRCHARTZ KR, SRULIJES JA & OERTEL Jr H. 1983. Steady and time-dependent Rayleigh-Bénard convection under influence of shear flows. Adv. Space Res., 3(5): 19–22.

LANDAU EM. 1944. On the problem of turbulence. C.R. Acad. Sci. URSS, 44: 311.

MALOMED BA and NEPOMNYASHCHY AA. 1993. Two-dimensional stability of convection rolls in the presence of a ramp. Europhys. Lett., 21(2): 195–200.

MALOMED BA, NEPOMNYASHCHY AA & TRIBELSKY MI. 1990. Domain boundaries in convection patterns. Phys. Rev. A, 41(12): 7244–7263.

MAMPAEY F. 1990. A stable alternating direction method for simulating multi-dimensional solidification problems. Int. J. Num. Meth. Engn., 30: 711–728.

MANNEVILLE P. 1990. Dissipative Structures and Weak Turbulence. Academic Press, San Diego.

MANNEVILLE P & POMEAU Y. 1983. A grain boundary in cellular structures near the onset of convection. Phil. Mag. A, 48: 607.

NORMAND C, POMEAU Y & VELARDE MG. 1977. Convective instability: A physicist's approach. Rev. Mod. Phys., 49: 581–624.

PEACEMAN DW & RACHFORD Jr HH. 1955. The numerical solution of paraboloic and eliptic differential equations. SIAM, 3: 28–41.

PONTES J. 1994. Pattern Formation in Spatially Ramped Rayleigh-Bénard Systems. PhD thesis, Université Libre de Bruxelles, Brussels.

PONTES J, CHRISTOV CI & VELARDE MG. 1996. Numerical study of patterns and their evolution in finite geometries. Int. J. Bifurcation and Chaos, 6(10): 1883–1890.

ROSENFELD M & YASSOUR Y. 1994. The alternating direction multizone implicit method. J. comp. Phys., 110: 212–220.

SRULIJES JA. 1979. Zellularkonvektion in Behältern mit Horizontalen Temperaturgradienten. PhD thesis, Fakultät für Maschinenbau, Univ. Karlsruhe, Karlsruhe.

SWIFT J & HOHENBERG PC. 1977. Hydrodynamic fluctuations at the convective instability. Phys. Rev. A, 15: 319–328.

VELARDE MG & NORMAND C. 1980. Convection. Sci. Am., 243: 92–108.

WALGRAEF D. 1997. Spatio-Temporal Pattern Formation. Springer, New York.

WALTON IC. 1982. On the onset of Rayleigh-Bénard convection in a fluid layer of slowly increasing depth. Stud. Appl. Maths., 67: 199–216.

WALTON IC. 1983. The onset of cellular convection in a shallow two-dimensional container of fluid heated non-uniformelly from below. J. Fluid Mech., 131: 455–470.

WESFREID J, POMEAU Y, DUBOIS M, NORMAND C & BERGÉ P. 1978. Critcal effects in Rayleigh-Bénard convection. J. Phys. Lett., 39 (7): 725–731.

YANENKO NN. 1971. The Method of Fractional Steps. Springer, New York.